ACS chemical biology

ACS AuthorChoice

Articles

pubs.acs.org/acschemicalbiology

Terms of Use

A Novel Paramagnetic Relaxation Enhancement Tag for Nucleic Acids: A Tool to Study Structure and Dynamics of RNA

Christoph H. Wunderlich,[†,‡] Roland G. Huber,[§,‡] Romana Spitzer,[†] Klaus R. Liedl,[§] Karin Kloiber,*[,†] and Christoph Kreutz*[,†]

[†]Institute of Organic Chemistry and Center for Molecular Biosciences Innsbruck (CMBI), University of Innsbruck, Innrain 80/82, 6020 Innsbruck, Austria

[§]Institute of General, Inorganic and Theoretical Chemistry and Center for Molecular Biosciences Innsbruck (CMBI), University of Innsbruck, Innrain 80/82, 6020 Innsbruck, Austria

Supporting Information

ABSTRACT: In this work, we present a novel 2,2,6,6-tetramethylpiperidine 1-oxyl (TEMPO) radical phosphoramidite building block, which can be attached to the 5′-terminus of nucleic acids. To investigate the paramagnetic relaxation enhancement (PRE) emanating from this radical center, we incorporated the TEMPO label into various types of RNAs. We measured proton PREs for selectively ^{13}C-isotope labeled nucleotides to derive long-range distance restraints in a short 15 nucleotide stem−loop model system, underscoring the potential of the 5′-TEMPO tag to determine long-range distance restraints for solution structure determination. We subsequently applied the distance-dependent relaxation enhancement induced by the nitroxide radical to discern two folding states in a bistable RNA. Finally, we investigated the fast conformational sampling of the HIV-1 TAR RNA, a paradigm for structural flexibility in nucleic acids. With PRE NMR in combination with molecular dynamics simulations, the structural plasticity of this RNA was analyzed in the absence and presence of the ligand L-argininamide.

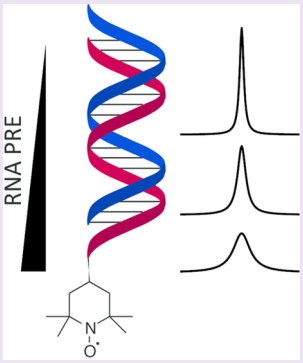

The structural and dynamic features of ribonucleic acids (RNA) are of central importance for exerting their manifold functions. Functional RNAs like ribozymes, riboswitches, or guide RNAs can fold into intricate three-dimensional architectures to which dynamics adds an additional layer of functional adaptability.[1−3] NMR spectroscopy has proven to be a powerful tool to determine the solution structure of RNA and RNA−RNA or RNA−protein complexes.[4−8] To this end and in analogy to protein NMR methods, classical structural NMR parameters, such as NOEs and scalar coupling restraints but also residual dipolar couplings (RDCs) are most commonly used. More recently, paramagnetic relaxation enhancement (PRE) NMR proved to be an extremely powerful tool for solution structure determination but also to probe dynamics in biological macromolecules.[9−11] PRE NMR is based on the introduction of a paramagnetic center, for example, an unpaired electron with an isotropic g-tensor like in nitroxide radicals or in the EDTA−Mn^{2+} complex. The experimental data yield long-range information arising from the r^{-6} distance dependence of the PRE effect. Furthermore, it can be exploited to address the structural plasticity of macromolecules fluctuating between transiently sampled excited states and a ground state.[12,13] Paramagnetic probes can be roughly divided into two classes: (i) nitroxide stable radicals and (ii) metal chelators (like EDTA, DPTA, or metal binding peptide), the latter binding paramagnetic metal ions with a very high affinity. As recently reported, paramagnetic cosolute molecules can be used for solution structure determination and to identify solvent accessible regions of the macromolecule surface.[14,15] The protocols for labeling proteins with paramagnetic tags are rather well established. For RNA, postsynthetic and direct synthetic labeling protocols using nitroxide radicals are established in the field of EPR spectroscopy.[16−21] Very recently, an approach using convertible nucleosides and DNA-catalyzed RNA ligation was introduced holding the promise to address larger RNAs, like riboswitch aptamer domains.[22] Some of these methods, however, might not be applicable for NMR spectroscopic applications due to issues concerning larger sample amounts in NMR spectroscopy, labeling efficiency, and chemical stability, reflected by the small number of RNA PRE NMR applications in the literature.[23,24] Here, we introduce a new phosphoramidite building block, **1**, which can be used to attach a nitroxide radical tag at the 5′-terminus of a nucleic acid. We demonstrate a range of possible applications of this PRE tag. In detail, we used a short hairpin construct to determine the potential of the 5′-radical moiety to derive long distance restraints, which represent valuable parameters in the solution structure determination process. For a bistable RNA, multiple stable folding states were assigned based on the PRE effect. Finally, transiently sampled conformational states for the HIV-1 TAR RNA were investigated in its uncomplexed form and bound to the ligand L-argininamide.

Received: August 5, 2013
Accepted: September 20, 2013
Published: September 20, 2013

Furthermore, we complemented our study with a molecular dynamic simulation of the HIV-1 TAR RNA.

RESULTS AND DISCUSSION

Synthesis of TEMPO Amidite 1 and Incorporation into RNA. With the commercially available 4-hydroxy-2,2,6,6-tetramethylpiperidine 1-oxyl, the desired phosphoramidite building block can be obtained in excellent yields (95%) by application of standard phosphitylation conditions. Further analytical data of **1** can be found in the Supporting Information (Supporting Figure 1a,b). The synthesis scheme of the nitroxide radical amidite **1** is shown below (Scheme 1). The obtained building block **1** is fully compatible with the RNA solid phase synthesis approach. As a proof of principle system, we chose a small, well-folded 15 nt hairpin RNA, **3**. The RNA was assembled under typical RNA solid phase conditions and the TEMPO amidite was attached at the 5′-terminus using standard conditions with the activator 5-benzylthio-1*H*-tetrazole and 2 min coupling time. Notably, there is no final detritylation step, because the TEMPO phosphoramidite **1** does not carry a trityl group (Scheme 2). Thus, in contrast to other approaches that use modified phosphoramidites to place labels at internal positions in the sequence, the nitroxide radical is not subjected to repeated detritylation and oxidation steps, which can lead to partial degradation of the radical moiety through a disproportionation mechanism.[25] Thus, despite of a lack in flexibility concerning sample design, 5′-tagging confers the advantage of chemical stability.

Scheme 1. One-Step Synthesis of the TEMPO Phosphoramidite 1[a]

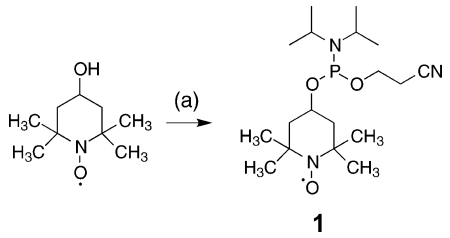

1

[a](2-Cyanoethyl)-*N*,*N*-diisopropyl chlorophosphoramidite (CEP-Cl), *N*-ethyldimethylamine (DMEA) in CH_2Cl_2, 30 min at rt, 95%.

Scheme 2. 5′-Tagging of Target RNAs with TEMPO Phosphoramidite 1[a]

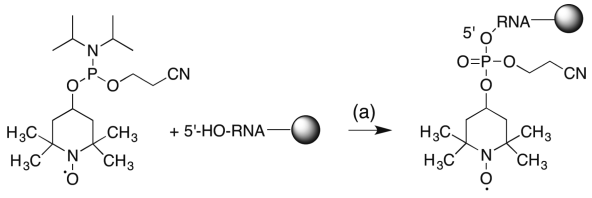

1

[a]5′-Benzylthio-1*H*-tetrazole in anhydrous acetonitrile, 2 min at rt, >98%, then capping A/B 1/1, 2 min at rt, then oxidation solution, 1 min at rt; then capping A/B 1/1, 2 min at rt. For the compositions of capping A and B and oxidation solution please refer to Materials and Methods section. The coupling of **1** was carried out on an ABI 391 DNA/RNA synthesizer.

We subsequently synthesized longer RNAs comprising 27 nt (**6**) and 32 nt (**5**). The anion-exchange chromatograms of the TEMPO labeled RNAs **3**, **5**, and **6** comprising site-specific ^{13}C-modifications are shown in the Supporting Information (Supporting Figure 1c). As judged from the HPLC traces, the TEMPO tag is incorporated at the 5′-terminus with at least 98% efficiency. By LC-MS, the integrity of the 15 nt hairpin RNA **3**, the 32 nt bistable RNA **5**, and the HIV-1 TAR RNA **6** all including the TEMPO tag was checked (Table 1). The accuracy of the reported mass data does not allow us to fully rule out the formation of traces of degraded TEMPO-tagged RNAs. However, from numerical simulations, we estimate that systematic errors arising from up to 10% diamagnetic impurities (in case of overlap of signals) on the extraction of distances is not exceeding experimental errors (Supporting Figure 1d, Supporting Information).

Table 1. Sequence Information and Analytical Data of the TEMPO-Modified RNA Sequences 3, 5, and 6

				molecular weight	
ID[a]	^{13}C-labels[b]	length[c]	yield,[d] nmol	calcd	found
3	4 (A, C, U)	15	527	5053.2	5052.2
5	1 (C)	32	502	10361.2	10361.7
6	8 (C)	27	480	8820.4	8820.2

[a]Sequence identifier. [b]Number of ^{13}C-labels (nucleotide type C = 6-^{13}C-cytidine, U = 6-^{13}C-uridine, A = 8-^{13}C-adenosine). [c]Number of nucleotides. [d]Yield from 2 μmol synthesis scale.

Read-out of PRE Data Using Site-Specifically Modified ^{13}C-RNAs. In principle, it would be possible to run PRE experiments on otherwise unlabeled RNA, either in a 1D or a 2D manner (via homonuclear scalar coupling or distance correlations). However, in this case one would lose important advantages characteristic to NMR isotope labeling schemes, like higher spectral resolution by isotope editing, or will be confronted with more complicated resonance assignment procedures due to spectral crowding in the proton chemical shift dimension. In analogy to procedures of protein NMR, uniform labeling with ^{15}N would yield AX spin systems at the imino sites of guanosine (G N^1–H) and uridine (U N^3–H). These protons are directly involved in hydrogen bonding and can be easily identified and assigned by their distinct chemical shift signature between 10 and 15 ppm and could potentially serve as read-out sites. The major drawback of using imino protons is their fast exchange with bulk solvent protons, a process that affects the magnetic history of the site (i.e., the read-out resonance carries information about the spectroscopic properties of water molecule, including relaxation rates) and introduces line broadening, which may be prohibitive for extracting reliable relaxation rates. Solvent exchange is found in double stranded regions leading to moderate (up to strong) line broadening and is most pronounced for single stranded regions rendering the nitrogen bound imino protons unobservable. Because the PRE effect is obtained by determining differences in the proton transverse relaxation rates, imino protons with their partially strongly enhanced line widths are not the most suitable reporter spins for extracting reliable PRE data.

For the purpose of extracting reliable information, it is desirable to work with sensitive, nonexchangeable spin systems with simple relaxation properties, such as AX spin systems in an otherwise magnetically dilute environment. Chemical synthesis of RNA via isotope-modified phosphoramidites is perfectly suited to achieve this goal. Here, we used ^{13}C–^{1}H groups in

dx.doi.org/10.1021/cb400589q | ACS Chem. Biol. 2013, 8, 2697–2706

nucleobases at chosen positions in the RNA sequence. These nonexchangeable protons present adequate spin systems for obtaining high quality paramagnetic relaxation data in both double and single stranded nucleic acid topologies. We earlier introduced 6-^{13}C-pyrimidine phosphoramidites to address conformational dynamics at the micro- to millisecond time regime using relaxation dispersion NMR.[26] Recently, we successfully expanded the repertoire of ^{13}C-modified RNA building blocks with 8-^{13}C-modified purine RNA phosphoramidites making it possible to freely choose the desired ^{13}C-labeling pattern as shown within this work (unpublished data). We found that these building blocks are also very useful to extract reliable relaxation enhancement effects induced by the TEMPO radical as exemplified by the three following examples.

Extraction of PRE Long-Range Distance Restraints for RNA Solution Structure Determination. The effect of paramagnetic relaxation enhancement not only depends on the distance between the paramagnetic center and the spin of interest but also on its time-modulation, which comprises the flexibility of both the spin and the radical tag. The PRE effect (otherwise extending to distances up to 30 Å) may be scaled down significantly by such structural flexibility. Since in our systems the radical is located at the 5′-end of the RNAs, which is a position with potentially higher flexibility (e.g., due to fraying of the terminal base pair or due to a single stranded 5′-terminal sequence region), we first used the rather static and well-defined 15 nucleotide hairpins **2** and **3** (Figure 1a) to test

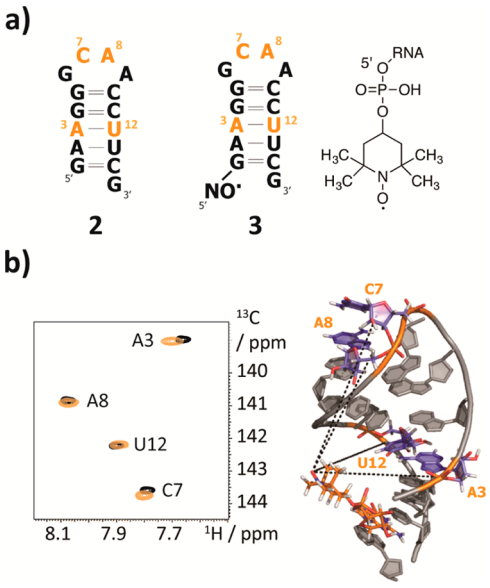

Figure 1. PRE for the determination of long-range distance restraints. (a) The 15 nt RNAs **2** and **3** and the 5′-TEMPO tag introduced via a phosphodiester bridge. The ^{13}C-modified nucleotides are highlighted in orange. (b) ^{1}H−^{13}C-HSQC spectra of RNA **2** (black) and **3** (orange). The PRE effect is most pronounced for residue A3. Structural model of the 15 nt RNA **3** visualizing the topology of the construct.

the range of distances within which the radical exerts its influence on nuclear spin relaxation. In detail, we labeled two nucleotides on opposite faces of the short stem as well as two nucleotides in the loop with ^{13}C at the C6 atomic position in pyrimidines (C7, U12) or C8 in purines (A3, A8), and equipped one of the samples with the TEMPO tag at the 5′-terminus. Each RNA molecule **2** and **3** thus contained four isolated ^{13}C−^{1}H spin systems whose proton transverse relaxation properties were determined via ^{13}C−^{1}H amplitude modulated correlation maps using an experiment previously published.[27] A superposition of spectra without and with TEMPO is shown (Figure 1b). The nitroxide spin label introduces slight variations in chemical shifts due to the slightly altered chemical environment, but neither the heteronuclear single quantum coherence (HSQC) nor the imino proton spectra indicated a perturbation of the general fold of hairpins **2** and **3** (Supporting Figure 2a,b, Supporting Information). The R_2 proton decays are shown in the Supporting Information (Supporting Figure 3a). For the hairpin RNA **2**, comprising well-known structure motifs, we obtained a structural model by using the MC-FOLD/MC-SYM pipeline, which was used to cross-validate our data.[28] The correlation time (τ_c) estimated by HydroPro NMR amounted to 3.2 ns. It turned out that the distances obtained from the experimental data are in very good agreement with the predicted structure (Table 2, Supporting Figure 3b, Supporting Information). The residue A3, which is the closest sequential and spatial neighbor of the TEMPO tag has a PRE of almost 30 s^{-1}, which corresponds to a distance of about 13 Å. We see nonzero PREs at all labeled ^{13}C-sites. This holds true even for C7 and A8, which are located in the extra-stable GNRA tetraloop that is about 20 Å away from the tag. The good agreement with predicted distances illustrates the potential of the label for implementation into 3D solution structure determination protocols for RNA and RNA−RNA or RNA−protein complexes.

Identification of Stable RNA Folding States. Model systems mimicking slowly interconverting RNA species, so-called bistable RNAs, were introduced by Micura and co-workers about 10 years ago.[29] For these RNAs, two competing secondary structure folds with nearly degenerate free energies are almost equally populated, their interconversion rates being so slow as to give rise to distinct peaks in NMR spectra (i.e., the chemical shift separation is much larger than the interconversion rate). Furthermore, if the interconversion rate is much slower than relaxation such that averaging of relaxation rates is inefficient, the two PRE effects from the two folds can be investigated separately. Thus, we used a 32 nt bistable RNA **5** bearing one cytidine 6-^{13}C-label, that is located at a position that is either close to (fold **5a**) or remote from (fold **5b**) the 5′-TEMPO tag (Figure 2a,b). Again, using one construct without the TEMPO label (bistable RNA **4**, Supporting Figure 2c, Supporting Information) and one equipped with the radical moiety (bistable RNA **5**), we found a PRE only for one of the folds (Figure 2c, Table 2), reflecting their significantly different distances to the radical center. From this data, unequivocal assignment of resonance C15a to fold **5a** is possible. This demonstrates that in larger RNAs where other NMR approaches (e.g., comparative imino proton approach) meet limitations PRE tagging is an option for fold assignments by NMR.

PRE To Study Fast Dynamics in the HIV-1 TAR RNA. As a final example, we wanted to address fast dynamics in RNA using the novel RNA PRE tagging methodology. A paradigm for such fast dynamics on the submicrosecond time scale is the HIV-1 transactivation response (TAR) RNA **6**. This viral RNA was extensively studied and undergoes rigorous conformational exchange on the fast NMR chemical shift time scale. The high degree of structural flexibility enables this RNA to bind various ligands, following a conformational selection mechanism.[30] In particular, the bulge UCU residues represent a dynamic

dx.doi.org/10.1021/cb400589q | ACS Chem. Biol. 2013, 8, 2697−2706

Table 2. PRE Data, Correlation Times (τ_c), PRE Effects, and PRE Derived and Predicted Distances of RNAs 3, 5, 6, and 6ARG

RNA ID[a]	residue[b]	PRE ^{1}H-Γ_2, s^{-1}[c]	correlation time (τ_c), ns[d]	distance (PRE), Å[e]	distance (predicted), Å[f]
3	A3	30.46 ± 1.51	3.2	13.2 ± 0.1	12.6
	C7	4.38 ± 0.79		18.3 ± 0.6	22.5
	A8	5.04 ± 0.78		17.7 ± 0.5	18.1
	U12	5.45 ± 0.82		17.6 ± 0.5	17.8
5	C15a	37.22 ± 2.83	*g*	*h*	*g*
	C15b	2.24 ± 2.78		*h*	*g*
6	C19	18.29 ± 2.39	4.71	15.29 ± 0.34	15.71 ± 1.30
	C24	*h*	3.69	*h*	29.32 ± 2.91
	C29	*h*	4.54	*h*	28.22 ± 4.76
	C33	2.67 ± 1.52	4.63	22.31 ± 4.42	34.05 ± 3.34
	C37	2.25 ± 1.36	4.34	23.11 ± 4.52	27.10 ± 4.39
	C39	3.94 ± 2.13	5.22	21.21 ± 4.40	19.97 ± 4.07
	C41	6.77 ± 2.51	5.27	18.97 ± 1.83	19.54 ± 3.17
	C44	14.80 ± 2.27	4.48	15.69 ± 0.37	17.84 ± 2.34
6ARG	C19	14.26 ± 2.16	4.64	15.92 ± 0.43	15.61 ± 1.49
	C24	0.93 ± 0.68	3.07	25.55 ± 5.12	31.76 ± 2.72
	C29	*h*	4.87	*h*	29.61 ± 4.07
	C33	*h*	4.62	*h*	34.49 ± 3.23
	C37	*h*	5.07	*h*	25.71 ± 3.91
	C39	10.87 ± 2.60	5.05	16.96 ± 0.75	19.73 ± 3.63
	C41	5.51 ± 2.85	4.73	19.82 ± 3.98	19.27 ± 3.17
	C44	8.28 ± 2.14	5.65	18.11 ± 0.90	17.79 ± 2.36

[a]RNA identifier. [b]A = adenosine; C = cytidine; U = uridine. [c]Paramagnetic relaxation enhancement effect determined as the difference between proton transverse relaxation rate from RNAs with and without TEMPO tag or by radical reduction using ascorbic acid (**6ARG**). [d]Correlation time estimates from HydroPro NMR[3] or from ^{13}C R_1 and $R_1\rho$ relaxation measurements (**6** and **6ARG**); [e]PRE derived distance. [f]Distances from structural model[3] or from molecular dynamic runs (**6** and **6ARG**). [g]Not available. [h]Not determined. Values with PRE error of 100% and more are considered insignificant and were not determined.

hotspot, where a large scale concerted bending and twisting of the upper and lower helix has been reported. Contrary to the previous case of the bistable RNA **5**, where the relaxation rates of two stable states were not disturbed by the slow exchange process, here one expects to find traces of the presence of transiently populated conformation states in the relaxation rates of an affected resonance. In the first place, we wanted to address the conformational heterogeneity of the free HIV-1 TAR RNA by determining the conformationally averaged PRE derived distances. Second, we used our approach to investigate the supposed rigidification of the molecule in the presence of the HIV-1 TAR RNA ligand argininamide and to pinpoint structural or dynamic changes upon binding in a site-resolved manner. To this end, we replaced all cytidine residues of a 27 nt HIV-1 TAR RNA mimic by the 6-^{13}C-modified counterparts and added a TEMPO moiety at the 5′-terminus yielding construct **6**. The ^{1}H−^{13}C-HSQC spectrum of this RNA **6** confirmed the preservation of the correct fold as only minor chemical shift deviations to the unmodified sequence were found (Figure 3a).

The PREs obtained on the sample in the absence of argininamide were detectable for nucleotides C19, C41, and C44 and to a smaller extent for C33, C37, and C39. For two residues, C24 and C29, no significant PRE effect was observed (Table 2). The immediate conclusion is that the two nucleotides (C19 and C44) that are spatially close (and located close to the 5′ and to the 3′ terminus, respectively) are strongly affected by the presence of the radical. The other nucleotides that exhibit a verifiable PRE are closer to the 3′-end of the RNA (C41, C39, and C37, in order of descending PRE) and in the loop (C33) (Supporting Figure 5a, Supporting Information). To translate the PRE effect into distances, we used the individual cytidine τ_c values (Table 2) determined from the ratio of the ^{13}C $R_1\rho/R_1$ rates (ranging from 3.96 to 5.27 ns, with an average of 4.61 ns).[31−33] We compared the PRE derived distances between the 5′-radical center and the H6 cytidine distances with mean values obtained from various HIV-1 TAR RNA structures deposited in the PDB comprising nine structures with different ligands bound (Supporting Table 1, Supporting Information). Noteworthy, a good correlation between the values was obtained for the averaged distances of the structure ensemble,[30] indicating that it is possible using PRE to pick up the signatures of transiently sampled states (Figure 4). Furthermore, it was earlier shown that MD simulations succeed to reproduce the conformational sampling of the free HIV-1 TAR RNA, like the concerted bending and twisting movement.[34,35] Thus, we decided to conduct a 1 μs MD simulation on the TEMPO tagged RNA **6**. In the simulation, the free RNA samples various distinct conformations in accordance with the earlier findings.[34] After about 100 ns, the free RNA relaxes from the ligand-bound template structure toward the free ensemble. Two distinct free conformations can be identified, with the high-energy conformation present around 10% of the time. Details of conformational sampling are given as two-dimensional RMSD plots in the Supporting Information (Supporting Figure 7a,b). The time-averaged H6-cytidine-TEMPO distances from this MD run are also in good agreement with the PRE-derived distances of the structural ensemble of the free RNA **6**. In particular, the residues close to the paramagnetic center are very well reproduced by the weighted arithmetic mean values of distances in the trajectory. The correlations of the PRE derived distances with the ones obtained from the PDB structure

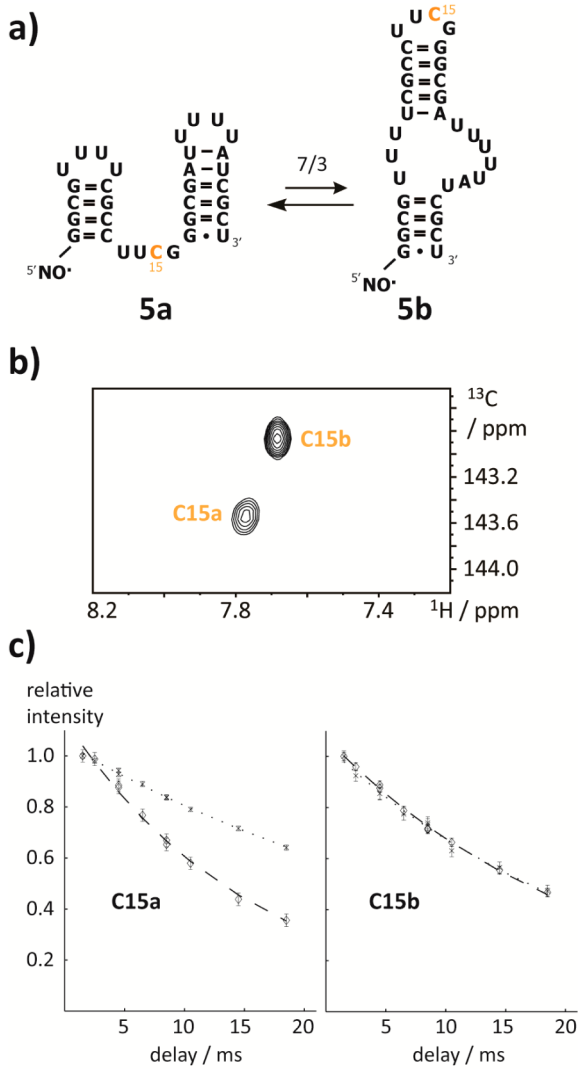

Figure 2. PRE in a bistable RNA. (a) Bistable RNA **5** with the proposed secondary structures **5a** and **5b** and the 6-^{13}C-cytidine highlighted in orange. (b) ^{1}H−^{13}C-HSQC spectrum of the TEMPO tagged RNA **5**. The resonance C15a shows a lower peak intensity compared with C15b. (c) Fold-differentiating PRE effect. Dotted and dashed lines represent R_2-decays without (bistable RNA **4**) and with (bistable RNA **5**) TEMPO tag, respectively. The individual folds are indicated. Errors are estimates from Monte Carlo analysis based on the signal-to-noise levels.

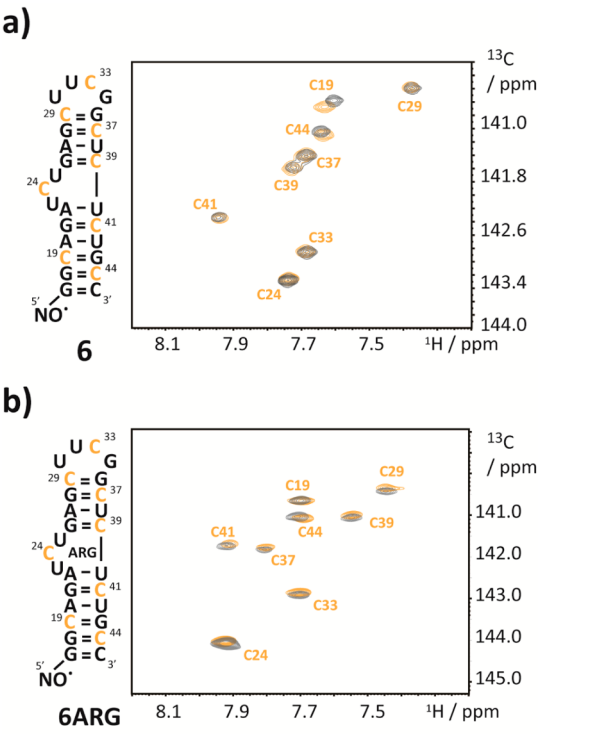

Figure 3. ^{1}H−^{13}C-HSQC spectra of TEMPO modified HIV-1 TAR RNA. (a) ^{1}H−^{13}C-HSQC-spectrum (orange) of HIV-TAR RNA **6** with 6-^{13}C-cytidine labels and a 5′-TEMPO tag. The corresponding spectrum of the unmodified sample is shown in black. (b) Same as in panel a but in the presence of 5 equiv of argininamide.

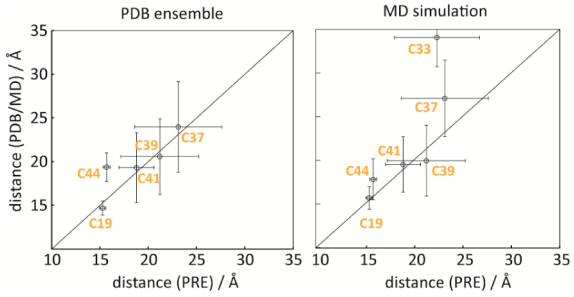

Figure 4. Distance correlation plots. Correlations between experimental distances of H6-^{13}C of cytidine residues from the radical center in the free HIV-1 TAR RNA **6** with the mean distance values obtained from an ensemble of structures of HIV-1 TAR RNA in complex with various ligands (left) and the time averaged values from the MD simulation (right). Error bars for the experimental values are derived from Monte Carlo analysis, whereas those for the structural ensemble and the MD simulation correspond to the standard deviations of the values. For residues C24 and C29, the errors in the PRE are more than 100%; thus the distance cannot be reliably extracted. Note that C33 (part of the non-natural extra-stable UUCG tetraloop) is missing in the PDB structure ensemble.

ensemble and those obtained from the MD simulation are shown (Figure 4).

One notable difference between PRE derived distances and MD derived distances is posed by C33, a nucleotide that is rather far away in the sequence but according to our experimental data seems to sample states of closer distance to the radical. This finding is in accordance with the large scale dynamical twisting and bending of the upper and lower stem.[30] The apparent discrepancy between the NMR and the molecular dynamics data is possibly a time frame issue. Whereas our MD run covers a trajectory of 1 μs, the PRE data are sensitive to dynamics occurring at various time scales ranging up to milliseconds and beyond.

Next we probed the effect of argininamide binding to HIV-1 TAR RNA **6** on the PRE. To saturate the binding pocket, we added a 5-fold excess of argininamide to the TEMPO tagged RNA **6** and an untagged analog. However, we were confronted with different line broadening effects arising from the residual exchange between the free and the ligand bound states in the two samples due to slight variations in the RNA/ligand stoichiometry (reported dissociation constants for the binding of argininamide to the HIV-1 TAR RNA range between 150 μM and 1 mM). This provided an additional source of different relaxation behavior between the two samples, and in turn, led to partially false (even negative) PRE effects and erroneous

dx.doi.org/10.1021/cb400589q | ACS Chem. Biol. 2013, 8, 2697−2706

distances. Thus, we performed a reduction step on the TEMPO labeled HIV-1 TAR RNA argininamide complex **6ARG** and compared proton relaxation rates obtained on one sample. We found that PREs that were strong in the free form were attenuated slightly (C19, C41, C44), quenched entirely (C33, C37), or increased (C39), pointing to a structural alteration due to ligand binding (Supporting Figure 6a,d). An MD simulation on the binary RNA–argininamide complex shows this conformation is preserved within the ligand-bound simulation. A second high-energy conformation is present in the ligand-bound simulation around 5% of the time. Details on the ligand-bound conformational ensemble as well as a detailed comparison with the free state conformational ensemble are given in the Supporting Information (Supporting Figures 8a,b and 9). The correlation of the experimentally derived averaged PRE distances with the MD trajectory derived time-averaged distances was again very good (Supporting Figure 6b,c, Supporting Information). The spatial approximation of C39, however, is not as pronounced in the MD simulation as implied by our experimental data. Two representative superpositions of histograms from the MD trajectory with experimental data before and after ligand binding are shown (Figure 5). In light of the previous experimental finding of rigidification of HIV-1 TAR RNA in the presence of argininamide, we tend to interpret our results in the sense that the bulge region adopts a more compact state (C39 comes closer to the 5′ end) and that the sampling of transient conformational states that include the UUCG loop residue C33 is arrested by ligand binding.[30]

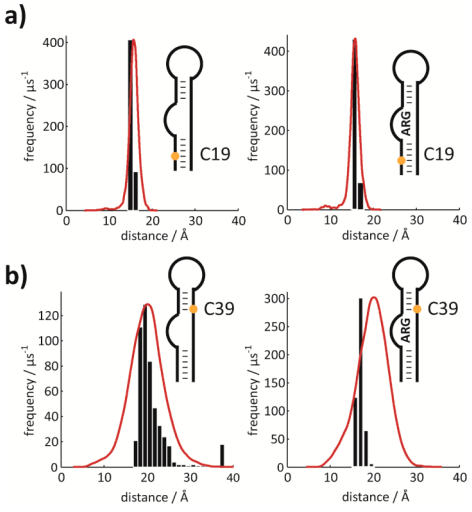

Figure 5. Comparison of MD/PRE derived distances. Comparison of histograms from MD simulations (red lines) with experimentally determined PRE derived distances (based on Monte Carlo simulations, black bar plots) of two representative nucleotides. (a) Results for C19 in free (left) and in the argininamide bound (right) state. (b) Results for C39 in free (left) and in the argininamide bound (right) state. Each histogram was constructed with the number of bins adjusted to the width of the sampled distances so as to give bars of the same width. The maxima of the MD distance distributions are normalized with respect to the maxima of the experimental distance distributions. Note that the distributions from the MD trajectory correspond to states that are actually sampled, whereas the distributions of experimental data are merely experimental errors of the mean values based on the signal-to-noise ratio in the spectra. Experimentally derived distances are a function of $PRE^{-1/6}$ resulting in a slight skew toward higher values even if PREs are equally distributed (simulations not shown).

Conclusions. We have introduced a labeling scheme that permits facile and reliable extraction of long distance restraints in well-structured RNA molecules. The approach is based on tagging of the 5′-terminus with a stable radical with a symmetric g-tensor using a TEMPO phosphoramidite derivative. Existing protocols use amino- or thioate-modified RNAs and a postsynthetic labeling step or, more recently, the convertible nucleoside approach or a labeling strategy based on click chemistry[18,22,23,36−38] to introduce the nitroxide label also at internal positions. Another synthetic route is represented by an enzymatic scheme,[36] where T7 RNA polymerase assisted transcription with guanosine monophosphorthioate priming was used to introduce a reactive sulfur center at the 5′ terminus, which can be modified with a spin label. A similar concept was reported by Qin and coworkers.[39] They used the T4 polynucleotide kinase to place a 5′-phosphorothioate group onto chemically and enzymatically synthesized RNAs. The sulfur was subsequently modified with an iodomethyl-modified nitroxide label.

Regarding the requirements for obtaining quantitative and reliable NMR data, our approach confers the important advantages over existing protocols of high sample amounts, homogeneity, and chemical stability. Furthermore, by our chemical synthesis, it is straightforward to combine the 5′-radical tag with other chemically modified labels of interest representing the sites that sense the 5′-tag and that can be freely chosen (as shown in our work). This is also of importance in NMR spectroscopic investigations for several practical reasons such as spectral crowding, relaxation properties of spin systems, or introducing various NMR-active nuclei. In addition, as the presented labeling scheme is fully compatible with internal radical tagging using either spin-labeled phosphoramidites or postsynthetic derivatization, RNA constructs suitable for advanced EPR methods could become feasible. Therefore we consider our synthetic solution a valuable expansion to existing protocols.

For reading out PREs, we used aromatic $^{13}C-^{1}H$ labeling at H6–C6 of pyrimidine and H8–C8 of purine nucleotides. These aromatic spin systems have the advantage of being dilute in terms of proton density, reducing the sources of side effects from scalar coupling or cross-correlated relaxation. The approach is nevertheless versatile with respect to the introduction of any other spin label, for example, fluorine-modified or 2′-*O*-$^{13}CH_3$ nucleotides.[40,41] It is of advantage to observe proton or fluorine PREs because their gyromagnetic ratios enter into the extent of the PRE effect.

We chose to determine the PRE from the difference of proton transverse relaxation rates (^{1}H-Γ_2) mainly for two reasons: (i) the ^{1}H-Γ_2 PRE is a highly sensitive probe due to the large gyromagnetic ratio of the proton and the dependence of ^{1}H-Γ_2 on the spectral density function at zero frequency and (ii) the transverse ^{1}H-Γ_2 rate is much less susceptible to internal dynamics and cross relaxation artifacts than the longitudinal PRE rate (^{1}H-Γ_1).[10]

To measure paramagnetic relaxation enhancement, we used mostly two samples that differed only in the presence of the radical tag in one of them (hairpin **2**/**3**, bistable RNA **4**/**5**). This approach works well for samples that are otherwise identical, such that no additional sources of differences in proton relaxation rates are present. It offers the advantage that the samples can be reused, in contrast to the approach commonly used for proteins, where the nitroxide radical is quenched by the addition of, for example, ascorbic acid.[42] We

dx.doi.org/10.1021/cb400589q | *ACS Chem. Biol.* 2013, 8, 2697–2706

worked at low sample concentrations (about 300−400 μM) compared with the standard sample amounts used in biomolecular NMR spectroscopy (i.e., 1 mM). Thereby constant relaxation rates are ensured, and the probability of intermolecular relaxation enhancement is reduced.

We used multipoint data to fit the exponential proton transverse relaxation decays and to extract the PRE effects. It is also possible to determine PRE from 2-point data.[10] However, because PRE effects are sometimes small, as in the case of the HIV-1 TAR RNA, we opted to acquire multipoint decays to increase the reliability of the data. Another experimental issue that has to be taken into account is the fact that the motional correlation time has to be determined (e.g., by $R_1/R_1\rho$ measurements) in order to extract reliable distance information. Because the PRE effect, via the spectral density functions, depends directly on τ_c (see Material and Methods section), the PRE derived distances show a $\tau_c^{1/6}$ dependence and are thus not extremely sensitive to experimental errors in correlation times (Supporting Figure 4, Supporting Information).

So far we could show that introduction of a single radical located at the 5′-end of the RNA is suitable for addressing structural and dynamic features of RNAs comprising up to 30 nucleotides. For NMR PRE studies on larger nucleic acids, internal radical labeling will become an inevitable challenge, which will be alleviated by NMR hardware advances (e.g., cryogenic probes) reducing the required sample amounts to low micromolar concentrations. Reliable information can be obtained for distances of up to about 20 Å for molecules with correlation times on the order of 4−6 ns. The dependence of the PRE on correlation time implies that for larger molecules, this limit is pushed to larger distances.

As a first application, we addressed the potential of the 5′ radical tag for the extraction of long-range distance restraints, which represent valuable parameters in the solution structure determination process. For that purpose, we chose a well-structured 15 nt hairpin RNA and found a very good agreement of PREs derived with modeled structure-based distances for this short RNA hairpin. One major concern regarding the suitability of our labeling scheme was the conformational flexibility of the 5′-end, which can, by reducing the observable PRE, severely compromise the extracted distance information. Note that in the 15 nt hairpin, the 5′-end is base-paired and further stabilized by a dangling 3′-nucleotide, keeping the intrinsic flexibility of the tag as low as possible. For the two other systems under investigation (bistable RNA **5** and HIV-TAR RNA **6**) the flexibility of the 5′-nitroxide moiety was restricted by attaching it to stems comprising at least four consecutive base pairs. The agreement of PRE- and structure-derived distances found for the short hairpin supports the notion that indeed in such a system the dynamics of the radical center is of minor importance. However, we expect that a longer, more flexible 5′-end will render the labeling scheme unsuitable for obtaining reliable PRE data.

As a second application, we have chosen a bistable RNA, as an example of structural heterogeneity. We obtained encouraging results in terms of discerning between different folds of a bistable RNA, where the PRE is unperturbed by the very slow dynamics of the system. As a final example, we investigated conformational dynamics in the fast exchange regime. We conducted PRE experiments on the HIV-1 TAR RNA, a well-known paradigm for RNA structural plasticity. The molecule is known to undergo large-scale dynamic reorientation of the upper and lower stem. Here, the PRE reflects an average value over all sampled conformations. We found indications for the sampling of multiple transient conformations in the free HIV-1 TAR RNA, which is important for this RNA to bind various ligands.[30] We were able to confirm the structural alterations induced by binding of argininamide.[43] The PRE based results are in good agreement with an MD trajectory conducted on HIV-1 TAR RNA **6** with and without argininamide bound, underscoring the potential of the approach in describing functionally important states in dynamic RNAs. Furthermore, the PRE data can be used to validate RNA MD simulations. Another, very exciting, application of the TEMPO tagged RNAs, which we will explore in the near future, is the NMR spectroscopic characterization of RNA−protein interactions.[44]

MATERIALS AND METHODS

Synthesis of TEMPO Amidite 1. *2,2,6,6-Tetramethylpiperidine 1-oxyl-4-O-(2′-cyanoethyl-N,N-diisopropylphosphoramidite) (1).* 4-Hydroxy-2,2,6,6-tetramethylpiperidine 1-oxyl (250 mg, 1.45 mmol, 1 equiv, Sigma Aldrich) was dissolved together with *N*-dimethylethylamine (1.06 g, 14.5 mmol, 10 equiv.) in 5 mL of absolute methylene chloride. After the solution was stirred for 15 min, 2-cyanoethyl-*N*,*N*-diisopropyl-chloro-phosphoramidite (412 mg, 1.74 mmol, 1.2 equiv) was added. After 30 min, the reaction mixture was diluted with methylene chloride and washed with half-saturated sodium bicarbonate solution. The organic phase was dried over sodium sulfate and evaporated to dryness. The crude product was purified by column chromatography on silica (ethyl acetate/hexanes 30/70 to 40/60 + 1% NEt_3) to give compound **1**. Yield: 515 mg (95%). TLC (ethyl acetate/hexanes 4/6): R_f = 0.45. ^{1}H NMR (300 MHz, $CDCl_3$, 25 °C): δ 0.94−1.55 (br, 24H); 2.77 (br, 4H); 3.63−4.10 (br, 8H) ppm. ^{31}P NMR (121 MHz, $CDCl_3$, 25 °C): δ 140.66 (br) ppm.

Synthesis of RNAs with 5′-TEMPO Tag. The TEMPO amidite **1** was used in combination with ^{13}C-modified phosphoramidites and with 2′-*O*-TOM protected building blocks (ChemGenes) to synthesize RNA sequences.[26] Custom primer support PS 200 (GE Healthcare) with an average loading of 80 μmol g^{-1} was used. The sequences were synthesized on an Applied Biossystems 391 PCR Mate using self-written RNA synthesis cycles. Amidite (0.1 M) and activator (5-benzylthio-1*H*-tetrazole, 0.25 M) solutions were dried over freshly activated molecular sieves overnight. The following reagents were used: detritylation solution, 4% dichloroacetic acid in 1,2-dichloroethane; capping A, 5.0 g of 4-(dimethylamino)-pyridine (DMAP) in 50 mL acetonitrile (0.5 M); capping B, 25 mL of acetonitrile, 15 mL of *sym*-collidine, and 10 mL of acetic anhydride (50/30/20); oxidation solution, 250 mg of iodine in 35 mL of THF, 10 mL of pyridine, and 5 mL of water.

The removal of protecting groups and the cleavage from solid support was achieved by treatment with aqueous methylamine (40%, 650 μL) and ethanolic methylamine (8 M, 650 μL) at RT for 6−8 h. After evaporation of the alkaline deprotection solution, the 2′-*O*-protecting groups were removed by adding 1 M TBAF (tetrabutylammonium fluoride) in THF (1200 μL). After 16 h at 310 K, the reaction was quenched by the addition of 1 M triethylammonium acetate (TEAA, pH 7.0, 1200 μL). The volume was reduced to approximately 1 mL and then applied on a HiPrep 26/10 desalting column (GE Healthcare). The crude RNAs were eluted with water, evaporated to dryness, and dissolved in 1 mL of water.

The quality of the crude RNAs was checked via anion exchange chromatography on a Dionex DNAPac PA-100 column (4 mm × 250 mm) using our standard eluents and at elevated temperature (80 °C). Purification of the RNA sequences was achieved by applying the crude RNA on a semipreparative Dionex DNAPac PA-100 column (9 mm × 250 mm). The fractions containing the desired RNA were pooled and loaded on a C18 SepPak cartridge (Waters) to remove HPLC buffer salts. The RNA triethylammonium salt form was then eluted from the C18 column with water/acetonitrile (1/1, v/v) and lyophilized. The integrity of the RNA was further checked by mass spectrometry on a

dx.doi.org/10.1021/cb400589q | ACS Chem. Biol. 2013, 8, 2697−2706

Finnigan LCQ Advantage MAX ion trap instrumentation connected to an Amersham Ettan micro LC (GE Healthcare).

NMR Spectroscopy. RNA samples were lyophilized as the triethylammonium salts and dissolved in the corresponding buffer in 9/1 H_2O/D_2O. The 15 nt hairpin RNAs **2** and **3** and the 32 nt bistable RNAs **4** and **5** were dissolved in 20 mM sodium cacodylate buffer, pH 6.4. The HIV-1 TAR RNA **6** was dissolved in 15 mM sodium phosphate buffer (pH 6.4) and 25 mM sodium chloride. Assignments were obtained by single ^{13}C-labeled RNAs (hairpin **2**/**3**) or by reference sequences (bistable RNA **4**/**5**) or were earlier reported (HIV-1 TAR RNA **6**/**6ARG**). Relaxation data in the absence and presence of the TEMPO tag were recorded either on two equivalent samples or before and after quenching the radical by addition of 1.5 equiv of ascorbic acid.[42] The RNA concentration in all experiments was equal to or lower than 0.4 mM to avoid intermolecular association events that could interfere with the PRE analysis. NMR experiments on the RNA sequences were conducted either on a Bruker 600 MHz Avance II+ instrument or on an Agilent DD2 instrument operating at 500 MHz proton larmor frequency. The 2D heteronuclear correlation spectra were processed using *NMRPipe* and visualized using *NMRDraw*.[45]

For determining the PRE effect, we used the difference in transverse proton relaxation rates (R_2) based on an earlier published pulse sequence.[27] The rates were determined from multipoint data recorded at 11.7 T at 298 K. For the 15 nt hairpin RNAs, the relaxation delays were set to 3, 6, 10, 16, 20, 28, 36, and 44 ms, the size of the data matrix was 1026 × 64 data points. For the 32 nt bistable RNAs, the relaxation delays were set to 3, 4, 6, 8, 10, 12, 16, and 20 ms with repeat experiments at 6 and 10 ms, with the 2048 × 48 complex data points. For the HIV-1 TAR RNAs, relaxation delays were set to 3, 4, 8, 12, 16, 24, and 32 ms with data sets of 2048 × 64 to 2048 × 96 complex points. The ^{13}C-R_1 and $R_1\rho$ experiments for the HIV-1 TAR RNA cytidines C6 were taken from the BioPack pulse sequence library. The ^{13}C-R_1 and $R_1\rho$ rates were determined at 11.7 T at 298 K. The relaxation delays were set to 0, 5, 10, 15, 20, 35, and 50 ($R_1\rho$) and 0, 20, 50, 100, 150, 200, and 300 ms (R_1), respectively. The typical size of the data matrices for relaxation data spectra was 2048 × 64 to 2048 × 80 complex data points. The number of scans was in a range between 32 and 128, and the interscan delay was 1.3 s to yield total measuring times of 16−24 h per experiment.

NMR Data Analysis. NMR spectra were analyzed using the *NMRPipe* and *NMRDraw* software packages.[45] The peak intensities from the ^1H T_2 experiments were determined by summing over an adequate grid of data points centered at the peak maxima. Subsequent steps were carried out using in-house written Matlab scripts (The MathWorks, www.mathworks.com).

The PRE is equivalent to the difference in proton transverse relaxation rates obtained by fitting monoexponential decays to data sets obtained on samples with and without TEMPO label. The experimental proton decays of transverse magnetization are well represented by a monoexponential function as relaxation pathways leading to cross-correlated relaxation are negligible to the sparseness of nearby NMR-active nuclei (in particular, CSA-DD H−CH cross-correlated relaxation appears to be very small). The PRE is translated into distance information using the following relations:

$$r = \left[\frac{K}{\mathrm{PRE}}(4J(0) + 3J(\omega_\mathrm{H}))\right]^{1/6}$$

$$J(\omega_i) = \frac{\tau_\mathrm{C}}{1 + (\omega_i\tau_\mathrm{C})^2}$$

$$\tau_\mathrm{C}^{-1} = \tau_\mathrm{R}^{-1} + \tau_\mathrm{e}^{-1} \approx \tau_\mathrm{R}^{-1}$$

where r is the distance between the paramagnetic center and the observed spin in cm and the constant K is given by

$$K = \frac{1}{15}S(S+1)(\mu_\mathrm{B}g_\mathrm{S}\gamma_\mathrm{I})^2 = 1.23 \times 10^{-32}\ \mathrm{cm}^6\ \mathrm{s}^{-2}$$

τ_c is the correlation time that determines the relevant spectral densities $J(\omega_i)$, which can be approximated by the motional correlation time of the molecule, τ_R, because the contribution of the electron relaxation time, τ_e, can be neglected ($\tau_e \gg \tau_R$). We used an estimate of the overall correlation time τ_R provided by the HydroPro NMR software for the 15 nt hairpin **3**.[46] For the 27 nt HIV-1 TAR RNA **6** and the argininamide complex **6ARG**, the correlation time (corresponding to the correlation time of overall molecular rotational motion with effects due to deviations from spherical symmetry of the molecular tumbling tensor or effects of intramolecular dynamics superimposed) was obtained from ^{13}C T_1 and $T_1\rho$ relaxation measurements according to Kay and co-worker.[31−33] Error estimates were obtained by Monte Carlo (MC) analysis (300−500 runs) based on noise estimates obtained from *NMRDraw*. The error propagates from $I(t)$ via the PRE to the distances. PREs with relative errors of more than 100% were considered insignificant.

Molecular Dynamics Simulations. Distance distributions were derived by microsecond molecular dynamics (MD) simulations of the HIV-1 TAR RNA with the TEMPO tag attached at the 5′-end. NMR structures of HIV-1 TAR RNA obtained by Davidson et al. retrieved from the Brookhaven PDB (PDB ID 2L8H) were used as a base template.[47] The loop sequence $C_{30}UGGGA_{35}$ was exchanged for a UCCG tetraloop obtained from PDB structure 2KOC by fitting the respective 3′- and 5′-ends and performing a local minimization for the two affected backbone phosphate groups using the MOE modeling package.[48] The loop exchange was performed in order to maintain consistency with the experimental construct. Electrostatic surface potentials were obtained for a methylphosphate-capped TEMPO moiety by *ab initio* calculations at the UHF/6-31G* level of theory and for the argininamide by HF/6-31G* using Gaussian 09. Subsequently, these potentials were used for fitting point charges using the RESP procedure as implemented in the AMBER package.[49] The nitroxide radical tag was covalently attached at the 5′-terminus of the TAR as a separate residue and subsequently minimized. The argininamide-bound state was obtained by modifying the arginine ligand in the 2L8H PDB structure. Parameter files for the TEMPO tag and the argininamide moiety are available on request. The TAR constructs were neutralized by sodium counterions to produce a net charge of zero for the entire system. Subsequently, all systems were solvated in an octahedral box of TIP3P water molecules with 12 Å wall separation. The parameter set χ0-YIL by Yildirim et al. was used to describe all RNA residues.[50] Equilibration comprised 500/500 steps of steepest descent/conjugate gradient minimization, followed by 100 ps NTP equilibration at a temperature of 300 K and 1 atm pressure, while keeping all heavy atoms restrained by a harmonic potential of 100 kcal/Å, followed by two separate runs of 500/500 minimization steps with restraint potentials of 10 kcal/Å and 1 kcal/Å, respectively. Then, 100 ps of unrestrained NTP equilibration concluded the system preparation phase. The 1 μs MD trajectories were obtained using the GPU implementation of *pmemd* with an integration time step of 0.2 fs and the SHAKE bond length constraints for all bonds to hydrogen atoms. Temperature and pressure were controlled by Langevin dynamics. Long-range electrostatics were described by the particle mesh Ewald procedure. Frames were stored at a 1 ps interval for analysis. RMSD and 2D-RMSD plots from the initial structures are given in the Supporting Information.

■ ASSOCIATED CONTENT

Ⓢ Supporting Information

Spectral data of TEMPO phosphoramidite **1** and analytical data of TEMPO modified RNA sequences **3**, **5**, and **6**, ^1H-NMR and HSQC spectra of hairpins **2** and **3** and bistable RNA **4** and **5** and references for fold assignment, R_2 proton decays of hairpin RNAs **2** and **3**, correlation of PRE derived distances versus distances from structural model of hairpin **3**, PRE derived distance variations from fluctuations in local cytidine correlation times, R_2 proton decays of the free HIV-1 TAR RNA **6** and binary HIV-1 TAR RNA argininamide complex

6ARG, MD distance distributions and PRE derived distances of the free HIV-1 TAR RNA **6** and binary HIV-1 TAR RNA argininamide complex **6ARG**, correlation of PRE derived distances versus MD time averaged distances of the binary HIV-1 TAR RNA argininamide complex **6ARG**, Analysis of the simulation of the TEMPO-tagged HIV-1 TAR RNA (**6**) and HIV-1 TAR RNA in complex with argininamide (**6ARG**), and comparison of the holo-HIV-1 TAR RNA (**6**) and the argininamide complex (**6ARG**) MD simulations. This material is available free of charge via the Internet at http://pubs.acs.org.

AUTHOR INFORMATION

Corresponding Authors

*Karin Kloiber. E-mail: karin.kloiber@uibk.ac.at. Telephone: +43 512 507 57730. Fax: +43 512 507 57799.

*Christoph Kreutz. E-mail: christoph.kreutz@uibk.ac.at. Telephone: +43 512 507 57725. Fax: +43 512 507 57799.

Author Contributions

‡C.H.W. and R.G.H. contributed equally.

Notes

The authors declare no competing financial interest.

ACKNOWLEDGMENTS

We thank R. Micura and R. Konrat for scientific discussions. This work was supported by the Tyrolean Science Fund TWF (Project 95421 to C.K.), the Austrian Science Fund FWF (Grant I844 to C.K., V173 to K.K.), and the CMBI scholarship (to R.S. and C.K.). R.S. and R.G.H. are recipients of a DOC Fellowship of the Austrian Academy of Sciences at the Institutes of Organic Chemistry and General, Inorganic and Theoretical Chemistry.

REFERENCES

(1) Wu, H., and Feigon, J. (2007) H/ACA small nucleolar RNA pseudouridylation pockets bind substrate RNA to form three-way junctions that position the target U for modification. *Proc. Natl. Acad. Sci. U. S. A. 104*, 6655−6660.

(2) Dethoff, E. A., Petzold, K., Chugh, J., Casiano-Negroni, A., and Al-Hashimi, H. M. (2012) Visualizing transient low-populated structures of RNA. *Nature 491*, 724−728.

(3) Reining, A., Nozinovic, S., Schlepckow, K., Buhr, F., Furtig, B., and Schwalbe, H. (2013) Three-state mechanism couples ligand and temperature sensing in riboswitches. *Nature 499*, 355−359.

(4) Dominguez, C., Schubert, M., Duss, O., Ravindranathan, S., and Allain, F. H. T. (2011) Structure determination and dynamics of protein−RNA complexes by NMR spectroscopy. *Prog. Nucl. Magn. Reson. Spectrosc. 58*, 1−61.

(5) Lu, K., Miyazaki, Y., and Summers, M. (2010) Isotope labeling strategies for NMR studies of RNA. *J. Biomol. NMR 46*, 113−125.

(6) Bothe, J. R., Nikolova, E. N., Eichhorn, C. D., Chugh, J., Hansen, A. L., and Al-Hashimi, H. M. (2011) Characterizing RNA dynamics at atomic resolution using solution-state NMR spectroscopy. *Nat. Methods 8*, 919−931.

(7) Duss, O., Lukavsky, P., and Allain, F. T. (2012) Isotope Labeling and Segmental Labeling of Larger RNAs for NMR Structural Studies, in *Isotope labeling in Biomolecular NMR* (Atreya, H. S., Ed.), pp 121−144, Springer, Dordrecht, the Netherlands.

(8) Santner, T., Rieder, U., Kreutz, C., and Micura, R. (2012) Pseudoknot Preorganization of the PreQ$_1$ Class I Riboswitch. *J. Am. Chem. Soc. 134*, 11928−11931.

(9) Clore, G. M., and Iwahara, J. (2009) Theory, Practice, and Applications of Paramagnetic Relaxation Enhancement for the Characterization of Transient Low-Population States of Biological Macromolecules and Their Complexes. *Chem. Rev. 109*, 4108−4139.

(10) Iwahara, J., Tang, C., and Marius Clore, G. (2007) Practical aspects of ^{1}H transverse paramagnetic relaxation enhancement measurements on macromolecules. *J. Magn. Reson. 184*, 185−195.

(11) Xue, Y., and Skrynnikov, N. R. (2011) Motion of a Disordered Polypeptide Chain as Studied by Paramagnetic Relaxation Enhancements, ^{15}N Relaxation, and Molecular Dynamics Simulations: How Fast Is Segmental Diffusion in Denatured Ubiquitin? *J. Am. Chem. Soc. 133*, 14614−14628.

(12) Iwahara, J., and Clore, G. M. (2006) Detecting transient intermediates in macromolecular binding by paramagnetic NMR. *Nature 440*, 1227−1230.

(13) Tang, C., Louis, J. M., Aniana, A., Suh, J.-Y., and Clore, G. M. (2008) Visualizing transient events in amino-terminal autoprocessing of HIV-1 protease. *Nature 455*, 693−696.

(14) Venditti, V., Niccolai, N., and Butcher, S. E. (2008) Measuring the dynamic surface accessibility of RNA with the small paramagnetic molecule TEMPOL. *Nucleic Acids Res. 36*, e20−e20.

(15) Madl, T., Bermel, W., and Zangger, K. (2009) Use of Relaxation Enhancements in a Paramagnetic Environment for the Structure Determination of Proteins Using NMR Spectroscopy. *Angew. Chem., Int. Ed. 48*, 8259−8262.

(16) Höbartner, C., Sicoli, G., Wachowius, F., Gophane, D. B., and Sigurdsson, S. T. (2012) Synthesis and Characterization of RNA Containing a Rigid and Nonperturbing Cytidine-Derived Spin Label. *J. Org. Chem. 77*, 7749−7754.

(17) Shelke, S. A., and Sigurdsson, S. T. (2010) Noncovalent and Site-Directed Spin Labeling of Nucleic Acids. *Angew. Chem., Int. Ed. 49*, 7984−7986.

(18) Edwards, T. E., and Sigurdsson, S. T. (2007) Site-specific incorporation of nitroxide spin-labels into 2′-positions of nucleic acids. *Nat. Protoc. 2*, 1954−1962.

(19) Krstić, I., Endeward, B., Margraf, D., Marko, A., and Prisner, T. (2012) Structure and Dynamics of Nucleic Acids, in *EPR Spectroscopy* (Drescher, M., and Jeschke, G., Eds.), pp 159−198, Springer, Berlin Heidelberg.

(20) Tkach, I., Pornsuwan, S., Hobartner, C., Wachowius, F., Sigurdsson, S. T., Baranova, T. Y., Diederichsen, U., Sicoli, G., and Bennati, M. (2013) Orientation selection in distance measurements between nitroxide spin labels at 94 GHz EPR with variable dual frequency irradiation. *Phys. Chem. Chem. Phys. 15*, 3433−3437.

(21) Krstić, I., Hänsel, R., Romainczyk, O., Engels, J. W., Dötsch, V., and Prisner, T. F. (2011) Long-Range Distance Measurements on Nucleic Acids in Cells by Pulsed EPR Spectroscopy. *Angew. Chem., Int. Ed. 50*, 5070−5074.

(22) Büttner, L., Seikowski, J., Wawrzyniak, K., Ochmann, A., and Höbartner, C. (2013) Synthesis of spin-labeled riboswitch RNAs using convertible nucleosides and DNA-catalyzed RNA ligation. *Bioorg. Med. Chem. 21*, 6171−6180.

(23) Qin, P. Z., Hideg, K., Feigon, J., and Hubbell, W. L. (2003) Monitoring RNA Base Structure and Dynamics Using Site-Directed Spin Labeling. *Biochemistry 42*, 6772−6783.

(24) Ramos, A., and Varani, G. (1998) A New Method To Detect Long-Range Protein−RNA Contacts: NMR Detection of Electron−Proton Relaxation Induced by Nitroxide Spin-Labeled RNA. *J. Am. Chem. Soc. 120*, 10992−10993.

(25) Rozantsev, E. G., and Sholle, V. D. (1971) Synthesis and Reactions of Stable Nitroxyl Radicals II. Reactions1. *Synthesis 1971*, 401−414.

(26) Wunderlich, C. H., Spitzer, R., Santner, T., Fauster, K., Tollinger, M., and Kreutz, C. (2012) Synthesis of (6-^{13}C)Pyrimidine Nucleotides as Spin-Labels for RNA Dynamics. *J. Am. Chem. Soc. 134*, 7558−7569.

(27) Iwahara, J., Schwieters, C. D., and Clore, G. M. (2004) Ensemble Approach for NMR Structure Refinement against ^{1}H Paramagnetic Relaxation Enhancement Data Arising from a Flexible Paramagnetic Group Attached to a Macromolecule. *J. Am. Chem. Soc. 126*, 5879−5896.

(28) Parisien, M., and Major, F. (2008) The MC-Fold and MC-Sym pipeline infers RNA structure from sequence data. *Nature 452*, 51−55.

(29) Höbartner, C., and Micura, R. (2003) Bistable Secondary Structures of Small RNAs and Their Structural Probing by Comparative Imino Proton NMR Spectroscopy. *J. Mol. Biol. 325*, 421−431.
(30) Zhang, Q., Stelzer, A. C., Fisher, C. K., and Al-Hashimi, H. M. (2007) Visualizing spatially correlated dynamics that directs RNA conformational transitions. *Nature 450*, 1263−1267.
(31) Kay, L. E., Torchia, D. A., and Bax, A. (1989) Backbone dynamics of proteins as studied by nitrogen-15 inverse detected heteronuclear NMR spectroscopy: application to staphylococcal nuclease. *Biochemistry 28*, 8972−8979.
(32) Gillespie, J. R., and Shortle, D. (1997) Characterization of long-range structure in the denatured state of staphylococcal nuclease. II. distance restraints from paramagnetic relaxation and calculation of an ensemble of structures. *J. Mol. Biol. 268*, 170−184.
(33) Gillespie, J. R., and Shortle, D. (1997) Characterization of long-range structure in the denatured state of staphylococcal nuclease. I. paramagnetic relaxation enhancement by nitroxide spin labels. *J. Mol. Biol. 268*, 158−169.
(34) Fulle, S., Christ, N. A., Kestner, E., and Gohlke, H. (2010) HIV-1 TAR RNA Spontaneously Undergoes Relevant Apo-to-Holo Conformational Transitions in Molecular Dynamics and Constrained Geometrical Simulations. *J. Chem. Inf. Model. 50*, 1489−1501.
(35) Zhang, Q., and Al-Hashimi, H. M. (2009) Domain-elongation NMR spectroscopy yields new insights into RNA dynamics and adaptive recognition. *RNA 15*, 1941−1948.
(36) Cekan, P., Smith, A. L., Barhate, N., Robinson, B. H., and Sigurdsson, S. T. (2008) Rigid spin-labeled nucleoside Ç: a nonperturbing EPR probe of nucleic acid conformation. *Nucleic Acids Res. 36*, 5946−5954.
(37) Piton, N., Mu, Y., Stock, G., Prisner, T. F., Schiemann, O., and Engels, J. W. (2007) Base-specific spin-labeling of RNA for structure determination. *Nucleic Acids Res. 35*, 3128−3143.
(38) Makino, K., Nagahara, S., Konishi, Y., Mukae, M., Ide, H., and Murakami, A. (1993) Detection of Specific Base Sequences in Solution Using DNA Probes Labeled with D- and/or ^{15}N-substituted Spin-labels. *Free Radical Res. 19*, s109−s116.
(39) Grant, G. P. G., and Qin, P. Z. (2007) A facile method for attaching nitroxide spin labels at the 5′ terminus of nucleic acids. *Nucleic Acids Res. 35*, No. e77.
(40) Kloiber, K., Spitzer, R., Tollinger, M., Konrat, R., and Kreutz, C. (2011) Probing RNA dynamics via longitudinal exchange and CPMG relaxation dispersion NMR spectroscopy using a sensitive ^{13}C-methyl label. *Nucleic Acids Res. 39*, 4340−4351.
(41) Fauster, K., Kreutz, C., and Micura, R. (2012) 2′-SCF_3 Uridine - A Powerful Label for Probing Structure and Function of RNA by ^{19}F-NMR Spectroscopy. *Angew. Chem., Int. Ed. 51*, 13080−13084.
(42) Xue, Y., Podkorytov, I. S., Rao, D. K., Benjamin, N., Sun, H., and Skrynnikov, N. R. (2009) Paramagnetic relaxation enhancements in unfolded proteins: Theory and application to drkN SH3 domain. *Protein Sci. 18*, 1401−1424.
(43) Pitt, S. W., Majumdar, A., Serganov, A., Patel, D. J., and Al-Hashimi, H. M. (2004) Argininamide Binding Arrests Global Motions in HIV-1 TAR RNA: Comparison with Mg^{2+}-induced Conformational Stabilization. *J. Mol. Biol. 338*, 7−16.
(44) Daubner, G. M., Cléry, A., and Allain, F. H. T. (2013) RRM−RNA recognition: NMR or crystallography...and new findings. *Curr. Opin. Struct. Biol. 23*, 100−108.
(45) Delaglio, F., Grzesiek, S., Vuister, G. W., Zhu, G., Pfeifer, J., and Bax, A. (1995) NMRPipe: a multidimensional spectral processing system based on UNIX pipes. *J. Biomol. NMR 6*, 277−293.
(46) Ortega, A., Amorus, D., and Garcia de la Torre, J. (2011) Prediction of Hydrodynamic and Other Solution Properties of Rigid Proteins from Atomic- and Residue-Level Models. *Biophys. J. 101*, 892−898.
(47) Davidson, A., Begley, D. W., Lau, C., and Varani, G. (2011) A Small-Molecule Probe Induces a Conformation in HIV TAR RNA Capable of Binding Drug-Like Fragments. *J. Mol. Biol. 410*, 984−996.
(48) Nozinovic, S., Fürtig, B., Jonker, H. R. A., Richter, C., and Schwalbe, H. (2010) High-resolution NMR structure of an RNA model system: the 14-mer cUUCGg tetraloop hairpin RNA. *Nucleic Acids Res. 38*, 683−694.
(49) Case, D. A., Cheatham, T. E., Darden, T., Gohlke, H., Luo, R., Merz, K. M., Onufriev, A., Simmerling, C., Wang, B., and Woods, R. J. (2005) The Amber biomolecular simulation programs. *J. Comput. Chem. 26*, 1668−1688.
(50) Yildirim, I., Stern, H. A., Kennedy, S. D., Tubbs, J. D., and Turner, D. H. (2010) Reparameterization of RNA χ Torsion Parameters for the AMBER Force Field and Comparison to NMR Spectra for Cytidine and Uridine. *J. Chem. Theory Comput. 6*, 1520−1531.